NJC

PAPER

View Article Online
View Journal | View Issue

Cite this: *New J. Chem.*, 2019, **43**, 755

Nitric oxide (NO) photo-release in a series of ruthenium–nitrosyl complexes: new experimental insights in the search for a comprehensive mechanism†

Max Roose, Marine Tassé, Pascal G. Lacroix * and Isabelle Malfant *

Received 3rd August 2018,
Accepted 28th November 2018

DOI: 10.1039/c8nj03907k

rsc.li/njc

A series of four ruthenium(II) complexes built from the $[Ru(terpy)(bipy)(NO)]^{3+}$ core (terpy is 2,2′:6′,2″-terpyridine and bipy is 2,2′-bipyridine) are investigated. They differ by the presence of zero, one, two, or three 4′-(4-methoxyphenyl) (MP) electron donor substituents introduced at different positions on the pyridine fragments to increase the intramolecular charge transfer capabilities towards the strongly withdrawing nitrosyl (NO) ligand. The UV-visible spectra reflect the presence and position of the MP substituents on the complexes. In the case of species containing the 4′-(MP)-terpy ligand, a low-lying transition is identified as arising from 4′-(MP)-terpy to Ru(NO) intramolecular charge transfer, which is further confirmed by TD-DFT analysis. Irradiation performed at λ = 436 nm on this isolated transition for different complexes leads to quantum yields of NO photo-release equal to 0.002 and 0.011, in a ratio of 6 (instead of 1), which allows concluding non-ambiguously that a single electron transition cannot account for the NO release mechanism.

Introduction

Nitric oxide ($NO^{\bullet}$) has been recognized as being involved in many biological functions such as blood pressure regulation, stimulation of immune response, neurotransmission and cytotoxic activity in tumor cells by apoptosis.[1,2] These numerous potential therapeutic actions have prompted research aimed at developing efficient $NO^{\bullet}$ donor molecules. Among them, ruthenium–nitrosyl [Ru(NO)] complexes are particularly appealing candidates in relation to their generally low toxicity, good chemical stability, and moreover their capability to release $NO^{\bullet}$ under light irradiation in the λ = 300–600 nm domain, exclusively,[3,4] taking advantage of the noninvasive and highly controllable characteristics of light, according to the following equation:

$$[Ru^{II}(NO^{+})] + \text{solvent} \xrightarrow{h\nu} [Ru^{III}(\text{solvent})] + NO^{\bullet} \qquad (1)$$

NO is a classic non-innocent ligand and metal–nitrosyls can have different electronic structure descriptions depending on their coordination environment. In the complexes here under investigation, the total number of electrons present in the ruthenium 3d orbitals and the π* orbitals of the nitrosyl ligand is equal to 6, which is written as $\{RuNO\}^6$ in the Enemark and Feltham notation which avoids the assignment of a formal oxidation state of the metal and a charge on the ligand.[5,6] However, it is reported that almost any $\{RuNO\}^6$ electronic configurations correspond to the formal $Ru^{II}NO^{+}$ electronic structure, which is EPR silent and in which the nitrosyl is regarded as a cation.[7] The presence of this resulting diamagnetic singlet ground state has been further supported by several computational studies.[8–11] Under these assumptions, the photo-release of the $NO^{\bullet}$ radical depicted in eqn (1) occurs after formal electron transfer to the nitrosyl ligand, achieved within an intense low-lying electron transition having a strong charge transfer character towards the strongly withdrawing nitrosyl, in all cases.

Several research teams have targeted $NO^{\bullet}$ donors in the class of ruthenium–bipyridine[12–14] and ruthenium–terpyridine[12a,15–17] complexes, built up from ligands of different donating/accepting capabilities. As a part of this research effort, we have recently reported on various ruthenium–nitrosyl complexes based on the $[Ru(tpy)(bpy)(NO)]^{3+}$ core[18] ($[RuT0B0]^{3+}$ in Scheme 1) initially investigated by Meyer *et al.*[19] (tpy stands for 2,2′:6′,2″-terpyridine and bpy for 2,2′-bipyridine). These various attempts were motivated by the idea that introducing a donor (either fluorene,[18a] carbazole,[18b] or methoxyphenyl[18c]) on the terpyridine ligand would favor intense charge transfer towards the RuNO fragment,

CNRS, LCC (Laboratoire de Chimie de Coordination), 205 route de Narbonne, 31077 Toulouse, France. E-mail: pascal.lacroix@lcc-toulouse.fr, isabelle.malfant@lcc-toulouse.fr

† Electronic supplementary information (ESI) available: ^{1}H NMR for the 6 Ru–X ruthenium complexes (X = Cl, NO_2, NO) with atom labeling, computational details (optimized structures and UV-visible spectra), and electrochemical and photorelease data for $[RuT1B0](PF_6)_3$ and $[RuT0B2](PF_6)_3$. ^{1}H-NMR-tracking of $NO^{\bullet}$ release from $[RuT1B2](PF_6)_3$. The IR spectrum for $[RuT1B2](PF_6)_3$ and its photoproduct. See DOI: 10.1039/c8nj03907k

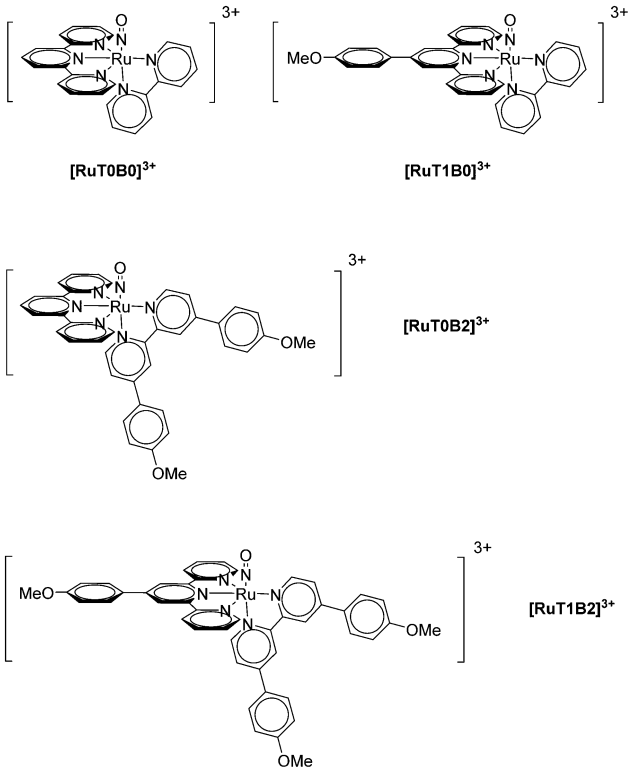

Scheme 1 [Ru(terpy)(bipy)(NO)]$^{2+}$ complexes with 0, 1, 2, and 3 methoxyphenyl substituents.

thus increasing the quantum yield of NO$^{\bullet}$ release (ϕ_{NO} = number of NO$^{\bullet}$ generated/number of photons absorbed by the complex).

In the present contribution, we wish to target the role of an electron donating substituent in the optical and photo-chemical properties of the ruthenium nitrosyl species through the investigation of a set of substitutions achieved either on the terpyridine ([RuT1B0]$^{3+}$), on the bipyridine ([RuT0B2]$^{3+}$), or on both ligands ([RuT1B2]$^{3+}$), as shown in Scheme 1. After the report and complete characterization of the ruthenium complexes, their optical spectra will be presented experimentally and approached computationally within the framework of density functional theory (DFT) to determine the origin of the observed transitions. ϕ_{NO} will be investigated by irradiation of the low-lying "push–pull" transitions, and tentatively analyzed in an attempt to provide new features towards a comprehensive description of the release process.

Experimental

Starting materials and equipment

The 4,4′-bis(4-methoxyphenyl)-2,2′-bipyridine (MP$_2$bipy)[20] and 4′-(4-methoxyphenyl)-2,2′:6′,2″-terpyridine (MPterpy)[21] ligands were synthesized as previously described in the literature. Likewise, [Ru(terpy)(Cl)$_3$] and [Ru(MPterpy)(Cl)$_3$] was synthetized following Adcock's procedure.[22] Triethylamine (Sigma-Aldrich), LiCl (Alfa Aesar), ethylene glycol (Fluka), NH_4PF_6 (Alfa Aesar), and $NaNO_2$ (Fluka) were the highest purity grade and were used as received. The ^{1}H NMR and ^{13}C NMR spectra were recorded at 298 K with a Bruker Avance 400 spectrometer, using $CDCl_3$, CD_3OD or CD_3CN as an internal reference. The IR spectra were recorded with a Perkin-Elmer (FTIR/FIR) 100 spectrometer. The ESI mass spectra were performed on a UPLC Xevo G2 Q TOF (Waters) spectrometer. The UV-vis spectra were obtained on a Perkin Elmer Lambda 35 UV-vis spectrometer. For the deconvolution of the spectra, the shapes of the transitions were assumed to correspond to Gaussian functions when drawn against the transition energies. Elemental analyses were performed at LCC with a Perkin-Elmer 2400 series II instrument. Electron paramagnetic resonance experiments (EPR) were performed on a Bruker ESP 500E spectrometer. The setup employed for the measurements was the same as that previously reported.[18c] [Fe(MGD)$_2$] (MGD = *N*-methyl-D-glucamine dithiocarbamate) was used as a spin trapping reagent.[23] The light source was a 250 W Oriel Hg lamp (Palaiseau, France).

Synthesis

The synthetic route towards [RuT0B2](PF$_6$)$_3$, and [RuT0B2](PF$_6$)$_3$ is summarized in Scheme 2. The atom labeling used for the ^{1}H- and ^{13}C-NMR assignments is provided as ESI† (Fig. S3).

[Ru^{II}(terpy)(MP$_2$bipy)Cl](Cl). [Ru^{III}(terpy)Cl$_3$] (88 mg, 0.2 mmol), MP$_2$bipy (74 mg, 0.2 mmol), lithium chloride (64 mg, 1.5 mmol), ethylene glycol (27 mL), and triethylamine (0.24 mL, 1.7 mmol) were successively added into a 50 mL flask. The mixture was heated at 160 °C for 4 h. After hot filtration, the mixture was evaporated to dryness under reduced pressure, at 120 °C. The residue obtained was washed with a large volume of water and sonicated, and finally filtered and dried under vacuum, providing 99 mg (64%) of the desired compound as a dark purple solid. ^{1}H NMR (CD_3OD, 400 MHz): δ 10.15 (1H, d, H_{6B}, $^3J_{6/5}$ = 6.0 Hz); 9.17 (1H, d, H_{3B}, $^4J_{3/5}$ = 2.0 Hz); 8.88 (1H, d, $H_{3'B}$, $^4J_{3'/5'}$ = 1.9 Hz); 8.66 (2H, d, $H_{3'T}$ + $H_{5'T}$, $^3J_{3'/4'}$ = $^3J_{5'/4'}$ = 8.1 Hz); 8.54 (2H, d, H_{3T} + $H_{3''T}$, $^3J_{3/4}$ = $^3J_{3''/4''}$ = 7.9 Hz); 8.28 (1H, dd, H_{5B}, $^3J_{5/6}$ = 6.1 Hz, $^4J_{5/3}$ = 1.9 Hz); 8.17–8.20 (2H, m, H_{2P} + H_{6P}); 8.14–8.17 (1H, t, $H_{4'T}$, $^3J_{4'/3'}$ = $^3J_{4'/5'}$ = 8.1 Hz); 7.94 (2H, td, H_{4T} + $H_{4''T}$, $^3J_{4/3}$ = $^3J_{4/5}$ = $^3J_{4''/3''}$ = $^3J_{4''/5''}$ = 7.9 Hz, $^4J_{4/6}$ = $^4J_{4''/6''}$ = 1.6 Hz); 7.82 (2H, m, H_{6T} + $H_{6''T}$); 7.77 (2H, m, $H_{2'P}$ + $H_{6'P}$); 7.36 (2H, m, H_{5T} + $H_{5''T}$); 7.28 (2H, m, $H_{5'B}$ + $H_{6'B}$); 7.23 (2H, m, H_{3P} + H_{5P}); 7.02 (2H, m, $H_{3'P}$ + $H_{5'P}$); 3.95 (3H, s, OCH_3); 3.82 (3H, s, OCH_3). ^{13}C NMR (CD_3OD, 100 MHz): δ 163.18 (C_{4P} or $C_{4'P}$); 163.05 (C_{4P} or $C_{4'P}$); 160.61 ($C_{2'B}$); 160.33 (C_{2T} + $C_{2''T}$); 159.65 ($C_{2'T}$ + $C_{6'T}$); 158.10 (C_{2B}); 153.47 (C_{6B}); 153.36 (C_{6T} + $C_{6''T}$); 152.48 ($C_{6'B}$); 149.94 (C_{4B}); 149.01 ($C_{4'B}$); 138.30 (C_{4T} + $C_{4''T}$); 135.22 ($C_{4'T}$); 130.04 (C_{2P} + C_{6P}); 129.86 (C_{1P}); 129.72 ($C_{2'P}$ + $C_{6'P}$); 129.13 ($C_{1'P}$); 128.56 (C_{5T} + $C_{5''T}$); 124.76 (C_{3T} + $C_{3''T}$); 124.69 (C_{5B}); 124.08 ($C_{5'B}$); 123.65 ($C_{3'T}$ + $C_{5'T}$); 121.48 (C_{3B}); 121.35 ($C_{3'B}$); 115.97 (C_{3P} + C_{5P}); 115.76 ($C_{3'P}$ + $C_{5'P}$); 55.34 (OCH_3); 55.24 (OCH_3). ESI-MS: *m*/*z*: 738.5 [M]$^+$.

[Ru^{II}(terpy)(MP$_2$bipy)(NO$_2$)](PF$_6$). [Ru^{II}(terpy)(MP$_2$bipy)(Cl)](Cl) (95 mg, 0.12 mmol) was dissolved in a mixture of ethanol (8.6 mL) and water (2.9 mL). After complete dissolution, $NaNO_2$ (83 mg, 1.2 mmol) was added and the violet resulting solution was heated under reflux for 3 h.[30] The solution turned dark red. After cooling down to room temperature, an excess of NH_4PF_6 (250 mg, 1.53 mmol) dissolved in 1 mL of water was added. The solution was concentrated to three-quarters of its volume and the resulting solution was cooled in a fridge overnight. After filtration and washing with cold water, a dark red solid was

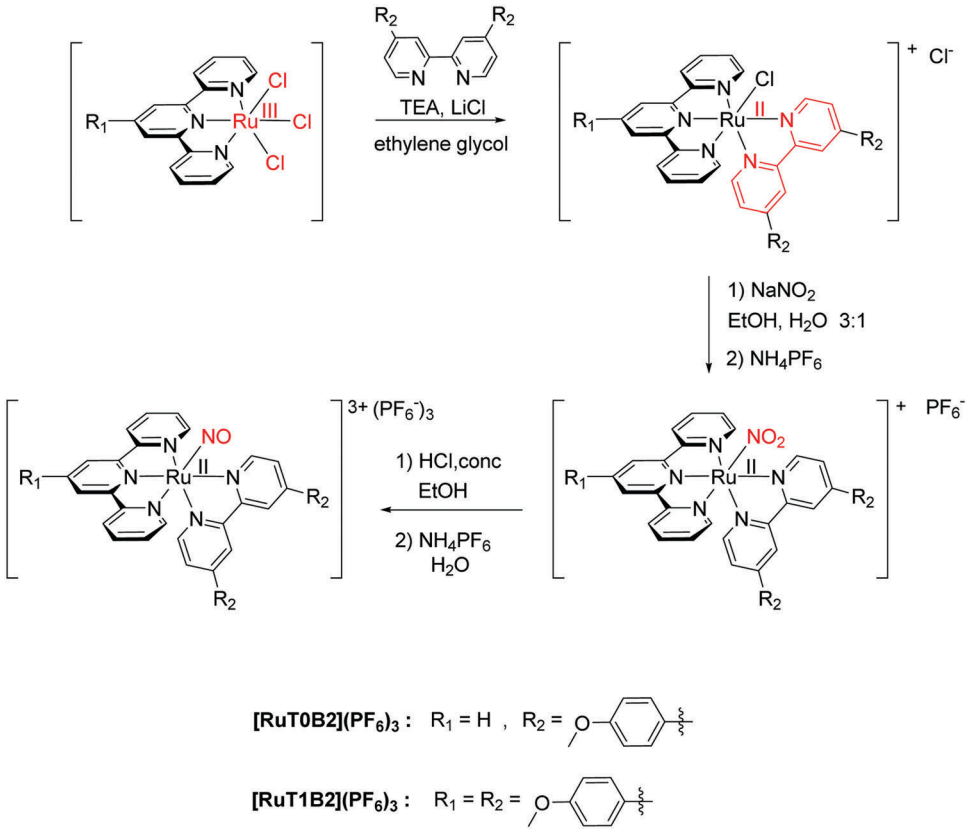

Scheme 2 Synthetic route towards $[RuT0B2](PF_6)_3$ and $[RuT1B2](PF_6)_3$.

dried under vacuum, affording 73 mg (68%) of the desired compound. ^{1}H NMR (CD_3CN, 400 MHz): δ 9.82 (1H, d, H_{6B}, $^3J_{6/5}$ = 6.1 Hz); 8.93 (1H, d, H_{3B}, $^4J_{3/5}$ = 2.0 Hz); 8.69 (1H, d, $H_{3'B}$, $^4J_{3'/5'}$ = 1.8 Hz); 8.49 (2H, d, $H_{3'T}$ + $H_{5'T}$, $^3J_{3'/4'}$ = $^3J_{5'/4'}$ = 8.0 Hz); 8.37 (2H, d, H_{3T} + $H_{3''T}$, $^3J_{3/4}$ = $^3J_{3''/4''}$ = 8.0 Hz); 8.21–8.16 (2H, m, H_{5B} + $H_{4'T}$); 8.10 (2H, m, H_{2P} + H_{6P}); 7.94 (2H, td, H_{4T} + $H_{4''T}$, $^3J_{4/3}$ = $^3J_{4/5}$ = $^3J_{4''/3''}$ = $^3J_{4''/5''}$ = 7.8 Hz, $^4J_{4/6}$ = $^4J_{4''/6''}$ = 1.5 Hz); 7.83 (2H, dd, H_{6T} + $H_{6''T}$, $^3J_{6/5}$ = $^3J_{6''/5''}$ = 5.5 Hz, $^4J_{6/4}$ = $^4J_{6''/4''}$ = 1.4 Hz); 7.74 (2H, m, $H_{2'P}$ + $H_{6'P}$); 7.34–7.22 (6H, m, H_{5T} + $H_{5''T}$ + $H_{5'B}$ + $H_{6'B}$ + H_{3P} + H_{5P}); 7.04 (2H, m, $H_{3'P}$ + $H_{5'P}$); 3.94 (3H, s, OCH_3); 3.83 (3H, s, OCH_3). ^{13}C NMR (CD_3CN, 100 MHz): δ 162.69 (C_{4P} ou $C_{4'P}$); 162.62 (C_{4P} ou $C_{4'P}$); 159.56 (C_{2T} + $C_{2''T}$); 159.09 ($C_{2'T}$ + $C_{6'T}$); 158.14 ($C_{2'B}$); 157.19 (C_{2B}); 153.70 (C_{6B}); 153.50 (C_{6T} + $C_{6''T}$); 151.81 ($C_{6'B}$); 149.50 ($C_{4'B}$); 149.20 (C_{4B}); 138.74 (C_{4T} + $C_{4''T}$); 136.40 ($C_{4'T}$); 129.91 (C_{2P} + C_{6P}); 129.84 ($C_{2'P}$ + $C_{6'P}$); 129.34 (C_{1P}); 128.72 ($C_{1'P}$); 128.44 (C_{5T} + $C_{5''T}$); 124.57 (C_{3T} + $C_{3''T}$ + C_{5B}); 123.73 ($C_{3'T}$ + $C_{5'T}$ + $C_{5'B}$); 121.57 (C_{3B}); 121.10 ($C_{3'B}$); 115.92 (C_{3P} + C_{5P}); 115.63 ($C_{3'P}$ + $C_{5'P}$); 56.34 (OCH_3); 55.24 (OCH_3). ESI-MS: m/z: 749.1 $[M]^+$; 372 $[M–NO_2 + CH_3CN]^{2+}$; 252. IR: ν (cm^{-1}): 1387 (ν_{NO_2}), 1346 (ν_{NO_2}), 839 (ν_{PF_6}), 558 (ν_{PF_6}).

$[RuT0B2](PF_6)_3$. $[Ru(terpy)(MP_2bipy)(NO_2)](PF_6)$ (75 mg, 0.083 mmol) was dissolved in a mixture of ethanol (30 mL) and HCl 37% (7 mL). The resulting dark red-brown solution was heated at 60 °C for 1 hour. The mixture was left at room temperature, and an excess of NH_4PF_6 (250 mg, 1.53 mmol) dissolved in 3 mL of water was added. The beginning of precipitation was noticed. The solution was put in a fridge for 2 h.[30] Filtrating, washing with cold water, and eventually drying under vacuum afforded 75 mg (77%) of a dark yellow solid. ^{1}H NMR (CD_3CN, 400 MHz): δ 9.23 (1H, d, H_{6B}, $^3J_{6/5}$ = 6.2 Hz); 9.16 (1H, d, H_{3B}, $^4J_{3/5}$ = 2.0 Hz); 9.00 (1H, m, $H_{4'T}$); 8.95–8.92 (3H, m, $H_{3'T}$ + $H_{5'T}$ + $H_{3'B}$); 8.76 (2H, d, H_{3T} + $H_{3''T}$, $^3J_{3/4}$ = $^3J_{3''/4''}$ = 7.9 Hz); 8.51–8.45 (3H, m, H_{4T} + $H_{4''T}$ + H_{5B}); 8.24 (2H, m, H_{2P} + H_{6P}); 8.17 (2H, dd, H_{6T} + $H_{6''T}$, $^3J_{6/5}$ = $^3J_{6''/5''}$ = 5.7 Hz, $^4J_{6/4}$ = $^4J_{6''/4''}$ = 1.4 Hz); 7.91 (2H, m, $H_{2'P}$ + $H_{6'P}$); 7.76 (2H, m, H_{5T} + $H_{5''T}$); 7.62 (1H, ddd, $H_{5'B}$, $^3J_{5'/4'}$ = 7.8 Hz, $^3J_{5'/6'}$ = 5.7 Hz, $^4J_{5'/3'}$ =1.3 Hz); 7.31 (2H, m, H_{3P} + H_{5P}); 7.13 (2H, m, $H_{3'P}$ + $H_{5'P}$); 7.11 (1H, m, $H_{6'B}$); 4.00 (3H, s, OCH_3); 3.97 (3H, s, OCH_3). ^{13}C NMR (CD_3CN, 100 MHz): δ 164.36 ($C_{4'P}$); 164.20 (C_{4P}); 157.6 (C_{2T} + $C_{2''T}$); 156.00 ($C_{2'B}$); 155.66 (C_{6T} + $C_{6''T}$); 155.57 (C_{2B} + $C_{4'B}$); 155.16 ($C_{2'T}$ + $C_{6'T}$); 154.69 (C_{4B}); 153.44 (C_{6B}); 148.31 ($C_{6'B}$); 147.90 ($C_{4'T}$); 145.36 (C_{4T} + $C_{4''T}$); 131.27 (C_{5T} + $C_{5''T}$); 131.01 (C_{2P} + C_{6P} ou $C_{2'P}$ + $C_{6'P}$); 130.95 (C_{2P} + C_{6P} ou $C_{2'P}$ + $C_{6'P}$); 128.66 (C_{3T} + $C_{3''T}$); 128.44 ($C_{3'T}$ + $C_{5'T}$); 127.28 (C_{1P}); 127.18 (C_{5B}); 126.74 ($C_{1'P}$); 126.24 ($C_{5'B}$); 124.34 (C_{3B}); 123.47 ($C_{3'B}$); 116.26 (C_{3P} + C_{5P}); 116.14 ($C_{3'P}$ + $C_{5'P}$); 56.54 (OCH_3); 56.52 (OCH_3). IR: ν (cm^{-1}): 1937 (ν_{NO}), 816 (ν_{PF_6}), 552 (ν_{PF_6}). ESI-MS: m/z: 360 $[Ru(terpy)(MP_2bpy)(H_2O)]^{2+}$; 372 $[Ru(terpy)(MP_2bpy)(CH_3CN)]^{2+}$; 749 $[Ru(terpy)(MP_2bpy)(NO_2)]^+$. UV-vis ($CH_3CN$): λ_{max} (ε): 229 nm (55 000 L mol^{-1} cm^{-1}), 292 nm (43 000 L mol^{-1} cm^{-1}), 322 nm (sh), 360 nm (33 000 L mol^{-1} cm^{-1}). Anal. calcd for $C_{39}H_{31}F_{18}N_6O_3P_3Ru$: C, 40.12; H, 2.68; N, 7.2. Found: C, 40.43; H, 2.34; N, 7.2.

$[Ru(MPterpy)(MP_2bipy)Cl](Cl)$. $[Ru(MPterpy)Cl_3]$ (137 mg, 0.25 mmol), MP_2bipy (92 mg, 0.25 mmol), lithium chloride (80 mg, 1.875 mmol [7.5 eq.]), ethylene glycol (29 mL), and

triethylamine (0.29 mL, 2.125 mmol) were successively introduced into a 50 mL flask. The mixture was heated at 170 °C for 8 h. After hot filtration, the solution was evaporated to dryness under reduced pressure at 120 °C. The residue obtained was washed with a huge amount of water and sonicated. The resulting dark purple solid was filtered, washed with water and a minimum of ethanol and ether, and dried under vacuum, affording 180 mg (82%) of the desired compound. ^{1}H NMR (CD_3OD, 400 MHz): δ 10.20 (1H, d, H_{6B}, $^3J_{6/5}$ = 6.0 Hz); 9.19 (1H, d, H_{3B}, $^4J_{3/5}$ = 1.9 Hz); 8.90 (3H, m, $H_{3'T}$ + $H_{5'T}$ + $H_{3'B}$); 8.69 (2H, d, H_{3T} + $H_{3''T}$, $^3J_{3/4}$ = $^3J_{3''/4''}$ = 7.9 Hz); 8.31 (1H, dd, H_{5B}, $^3J_{5/6}$ = 6.2 Hz, $^4J_{5/3}$ = 1.9 Hz); 8.21 (2H, d, H_{2Pb} + H_{6Pb}, $^3J_{2/3}$ = $^3J_{6/5}$ = 8.4 Hz); 8.15 (2H, d, H_{2Pt} + H_{6Pt}, $^3J_{2/3}$ = $^3J_{6/5}$ = 8.3 Hz); 7.93 (2H, m, H_{4T} + $H_{4''T}$); 7.84 (2H, d, H_{6T} + $H_{6''T}$, $^3J_{6/5}$ = $^3J_{6''/5''}$ = 5.4 Hz); 7.79 (2H, d, $H_{2'Pb}$ + $H_{6'Pb}$, $^3J_{2'/3'}$ = $^3J_{6'/5'}$ = 8.5 Hz); 7.38–7.36 (3H, m, $H_{6'B}$ + H_{5T} + $H_{5''T}$); 7.31–7.29 (1H, m, $H_{5'B}$); 7.26–7.21 (4H, m, H_{3Pb} + H_{5Pb} + H_{3Pt} + H_{5Pt}); 7.04 (2H, m, $H_{3'Pb}$ + $H_{5'Pb}$, $^3J_{3'/2'}$ = $^3J_{5'/6'}$ = 8.5 Hz); 3.97 (3H, s, OCH_3); 3.96 (3H, s, OCH_3); 3.84 (3H, s, OCH_3). ^{13}C NMR (CD_3OD, 100 MHz): δ 161.79 (C_{4Pb}); 161.65 ($C_{4'Pb}$); 161.59 (C_{4Pt}); 159.31 ($C_{2'B}$); 159.18 (C_{2T} + $C_{2''T}$); 158.13 ($C_{2'T}$ + $C_{6'T}$); 156.82 (C_{2B}); 152.12 (C_{6B}); 152.00 (C_{6T} + $C_{6''T}$); 151.09 ($C_{6'B}$); 148.43 (C_{4B}); 147.52 ($C_{4'B}$); 146.55 ($C_{4'T}$); 136.80 (C_{4T} + $C_{4''T}$); 128.95 (C_{1Pt}); 128.63 (C_{2Pt} + C_{6Pt} + C_{2Pb} + C_{6Pb}); 128.50 (C_{1Pb}); 128.30 ($C_{2'Pb}$ + $C_{6'Pb}$); 127.78 ($C_{1'Pb}$); 127.04 (C_{5T} + $C_{5''T}$); 123.54 (C_{3T} + $C_{3''T}$); 123.26 (C_{5B}); 122.67 ($C_{5'B}$); 120.07 (C_{3B}); 119.92 ($C_{3'B}$); 119.29 ($C_{3'T}$ + $C_{5'T}$); 114.57 (C_{3Pb} + C_{5Pb} or C_{3Pt} + C_{5Pt}); 114.55 (C_{3Pb} + C_{5Pb} or C_{3Pt} + C_{5Pt}); 114.34 ($C_{3'Pb}$ + $C_{5'Pb}$); 54.63 (OCH_3 × 2); 54.51 (OCH_3). ESI-MS: m/z: 844.4 $[M]^+$.

[Ru(MPterpy)(MP$_2$bipy)(NO$_2$)](PF$_6$). [Ru(MPterpy)(MP$_2$bpy)(Cl)]Cl (130 mg, 0.15 mmol) was dissolved in a mixture of ethanol (12 mL) and water (4 mL). $NaNO_2$ (96 mg, 1.40 mmol) was added and the reaction mixture was heated under reflux for 4 h.[20] The dark brown solution was cooled down to room temperature, and an excess of NH_4PF_6 (350 mg, 2.1 mmol) dissolved in 1 mL of water was added. The solution was concentrated to three-quarters of its volume, and the resulting solution was cooled in a fridge for 1 h. After filtration and washing with cold water, the resulting dark brown solid was dried under vacuum in a desiccator. The crude compound (138 mg) was purified as follows: the solid was dissolved in 135 mL of dichloromethane and the solution was filtrated. Petroleum ether (550 mL) was slowly added to the filtrate under stirring. The resulting mixture was put in a freezer for 3 h. Filtrating, washing with cold petroleum ether and drying under vacuum provided 93 mg (62%) of the desired compound, as a brown solid. ^{1}H NMR (CD_3CN, 400 MHz): δ 9.87 (1H, d, H_{6B}, $^3J_{6/5}$ = 6.0 Hz); 8.97 (1H, d, H_{3B}, $^4J_{3/5}$ = 2.0 Hz); 8.73 (1H, d, $H_{3'B}$, $^4J_{3'/5'}$ = 2.0 Hz); 8.71 (2H, s, $H_{3'T}$ + $H_{5'T}$); 8.50 (2H, m, H_{3T} + $H_{3''T}$); 8.23 (1H, dd, H_{5B}, $^3J_{5/6}$ = 6.1 Hz, $^4J_{5/3}$ = 2.0 Hz); 8.14 (2H, m, H_{2Pb} + H_{6Pb}); 8.10 (2H, m, H_{2Pt} + H_{6Pt}); 7.96 (2H, td, H_{4T} + $H_{4''T}$, $^3J_{4/3}$ = $^3J_{4/5}$ = $^3J_{4''/3''}$ = $^3J_{4''/5''}$ = 7.9 Hz, $^4J_{4/6}$ = $^4J_{4''/6''}$ = 1.6 Hz); 7.88 (2H, m, H_{6T} + $H_{6''T}$); 7.77 (2H, m, $H_{2'Pb}$ + $H_{6'Pb}$); 7.39–7.33 (3H, m, $H_{6'B}$ + H_{5T} + $H_{5''T}$); 7.30–7.23 (5H, m, $H_{5'B}$ + H_{3Pb} + H_{5Pb} + H_{3Pt} + H_{5Pt}); 7.06 (2H, m, $H_{3'Pb}$ + $H_{5'Pb}$); 3.97 (6H, s, OCH_3 × 2); 3.85 (3H, s, OCH_3). ^{13}C NMR (CD_3CN, 100 MHz): δ 161.71 (C_{4Pb} or $C_{4'Pb}$ or C_{4Pt}); 161.61 (C_{4Pb} or $C_{4'Pb}$ or C_{4Pt}); 161.60 (C_{4Pb} or $C_{4'Pb}$ or C_{4Pt}); 158.79 (C_{2T} + $C_{2''T}$); 157.91 ($C_{2'T}$ + $C_{6'T}$); 157.23 ($C_{2'B}$); 156.28 (C_{2B}); 152.70 (C_{6B}); 152.58 (C_{6T} + $C_{6''T}$); 150.74 ($C_{6'B}$); 148.47 ($C_{4'B}$); 148.11 (C_{4B}); 147.43 ($C_{4'T}$); 137.63 (C_{4T} + $C_{4''T}$); 129.10 (C_{2Pt} + C_{6Pt}); 129.00 (C_{1Pt}); 128.91 (C_{2Pb} + C_{6Pb} or $C_{2'Pb}$ + $C_{6'Pb}$); 128.86 (C_{2Pb} + C_{6Pb} or $C_{2'Pb}$ + $C_{6'Pb}$) 128.38 (C_{1Pb}); 127.76 ($C_{1'Pb}$); 127.35 (C_{5T} + $C_{5''T}$); 123.63 (C_{3T} + $C_{3''T}$); 123.59 (C_{5B}); 122.73 ($C_{5'B}$); 120.57 (C_{3B}); 120.11 ($C_{3'B}$); 120.01 ($C_{3'T}$ + $C_{5'T}$); 114.93 (C_{3Pb} + C_{5Pb} or C_{3Pt} + C_{5Pt}); 114.86 (C_{3Pb} + C_{5Pb} or C_{3Pt} + C_{5Pt}); 114.63 ($C_{3'Pb}$ + $C_{5'Pb}$); 55.35 (OCH_3 × 2); 55.24 (OCH_3). IR: ν (cm^{-1}): 1334 (ν_{NO_2}), 843 (ν_{PF_6}), 826 (ν_{PF_6}), 557 (ν_{PF_6}). ESI-MS: m/z: 855.2 $[M]^+$.

[RuT1B2](PF$_6$)$_3$. [Ru(MPterpy)(MP$_2$bipy)(NO$_2$)](PF$_6$) (60 mg, 0.060 mmol) was dissolved in a mixture of ethanol (22.5 mL) and HCl 37% (5 mL). The resulting brown solution was heated at 60 °C for 1 h. The solution was left to cool to room temperature, and an excess of NH_4PF_6 (350 mg, 2.13 mmol) dissolved in 3 mL of water was added. The resulting solution was evaporated under vacuum at a temperature maintained below 30 °C, until the beginning of precipitation occurred. The mixture was put in a fridge overnight. After filtration and washing with cold water, the resulting dark orange solid was dried under vaccum (72 mg, 94%). ^{1}H NMR (CD_3CN, 400 MHz): δ 9.23 (1H, d, H_{6B}, $^3J_{6/5}$ = 6.2 Hz); 9.13 (1H, d, H_{3B}, $^4J_{3/5}$ = 2.1 Hz); 9.08 (2H, s, $H_{3'T}$ + $H_{5'T}$); 8.92–8.89 (3H, m, $H_{3'B}$ + H_{3T} + $H_{3''T}$); 8.51 (2H, td, H_{4T} + $H_{4''T}$, $^3J_{4/3}$ = $^3J_{4/5}$ = $^3J_{4''/3''}$ = $^3J_{4''/5''}$ = 7.9 Hz, $^4J_{4/6}$ = $^4J_{4''/6''}$ = 1.5 Hz); 8.47 (1H, dd, H_{5B}, $^3J_{5/6}$ = 6.2 Hz, $^4J_{5/3}$ = 2.1 Hz); 8.32 (2H, m, H_{2Pt} + H_{6Pt}); 8.23 (2H, m, H_{2Pb} + H_{6Pb}); 8.17 (1H, dd, H_{6T} + $H_{6''T}$, $^3J_{6/5}$ = $^3J_{6''/5''}$ = 5.6 Hz, $^4J_{6/4}$ = $^4J_{6''/4''}$ = 1.4 Hz); 7.90 (2H, m, $H_{2'Pb}$ + $H_{6'Pb}$); 7.76 (2H, m, H_{5T} + $H_{5''T}$); 7.62 (1H, dd, $H_{5'B}$, $^3J_{5'/6'}$ = 6.4 Hz, $^4J_{5'/3'}$ = 2.1 Hz); 7.36 (2H, m, H_{3Pt} + H_{5Pt}); 7.31 (2H, m, H_{3Pb} + H_{5Pb}); 7.24 (1H, d, $H_{6'B}$, $^3J_{6'/5'}$ = 6.4 Hz); 7.13 (2H, m, $H_{3'Pb}$ + $H_{5'Pb}$); 4.02 (3H, s, OCH_3); 4.00 (3H, s, OCH_3); 3.89 (3H, s, OCH_3). ^{13}C NMR (CD_3CN, 100 MHz): δ 163.90 (C_{4Pt}); 163.37 ($C_{4'Pb}$); 163.22 (C_{4Pb}); 158.07 ($C_{4'T}$); 156.90 (C_{2T} + $C_{2''T}$); 154.99 ($C_{4'B}$); 154.63 (C_{6T} + $C_{6''T}$ + $C_{2'B}$); 154.54 (C_{4B}); 153.68 ($C_{2'T}$ + $C_{6'T}$); 153.61 (C_{2B}); 152.33 (C_{6B}); 147.34 ($C_{6'B}$); 144.25 (C_{4T} + $C_{4''T}$); 130.58 (C_{2Pt} + C_{6Pt}); 130.10 (C_{5T} + $C_{5''T}$); 130.00 (C_{2Pb} + C_{6Pb} or $C_{2'Pb}$ + $C_{6'Pb}$); 129.93 (C_{2Pb} + C_{6Pb} or $C_{2'Pb}$ + $C_{6'Pb}$); 127.48 (C_{3T} + $C_{3''T}$); 126.63 (C_{1Pt}); 126.30 (C_{1Pb}); 126.21 (C_{5B}); 125.76 ($C_{1'Pb}$); 125.25 ($C_{5'B}$); 123.53 ($C_{3'T}$ + $C_{5'T}$); 123.28 (C_{3B}); 122.42 ($C_{3'B}$); 115.54 (C_{3Pt} + C_{5Pt}); 115.28 (C_{3Pb} + C_{5Pb}); 115.14 ($C_{3'Pb}$ + $C_{5'Pb}$); 55.73 (OCH_3); 55.58 (OCH_3); 55.52 (OCH_3). IR: ν (cm^{-1}): 1933 (ν_{NO}), 829 (ν_{PF_6}), 556 (ν_{PF_6}). ESI-MS: m/z: 855.2 $[Ru^{II}(MPterpy)(MP_2bipy)(NO_2)]^+$; 425.1 $[Ru^{II}(MPterpy)(MP_2bipy)(CH_3CN)]^{2+}$; 419.6 $[Ru^{II}(MPterpy)(MP_2bipy)(NO^{\bullet})]^{2+}$; 413.6 $[Ru^{II}(MPterpy)(MP_2bipy)(H_2O)]^{2+}$; 404.6 $[Ru^{II}(MPterpy)(MP_2bpy)]^{2+}$; 283.4 $[Ru^{III}(MPterpy)(MP_2bpy)(CH_3CN)]^{3+}$; 269.4 $[Ru^{III}(MPterpy)(MP_2bpy)]^{3+}$. UV-Vis ($CH_3CN$): λ_{max} (ε): 227 (52 000 L mol^{-1} cm^{-1}), 275 (sh), 291 (51 000 L mol^{-1} cm^{-1}), 315 (sh), 365 (39 000 L mol^{-1} cm^{-1}), 440 (sh). Anal. calcd for $C_{46}H_{37}F_{18}N_6O_4P_3Ru$: C, 43.37; H, 2.93; N, 6.6. Found: C, 43.25; H, 2.69; N, 6.47.

[Ru(terpy)(MP$_2$bipy)(CH$_3$CN)](PF$_6$)$_2$. ^{1}H NMR (CD_3CN, 400 MHz): δ 9.55 (1H, d, H_{6B}, $^3J_{6/5}$ = 6.0 Hz); 8.97 (1H, d, H_{3B}, $^4J_{3/5}$ = 2.0 Hz); 8.70 (1H, d, $H_{3'B}$, $^4J_{3'/5'}$ = 2.1 Hz); 8.58 (2H, d, $H_{3'T}$ + $H_{5'T}$, $^3J_{3'/4'}$ = $^3J_{5'/4'}$ = 8.1 Hz); 8.44 (2H, m, H_{3T} + $H_{3''T}$); 8.32 (1H, t, $H_{4'T}$, $^3J_{4'/3'}$ = $^3J_{4'/5'}$ = 8.1 Hz); 8.19 (1H, dd, H_{5B},

$^3J_{5/6}$ = 6.0 Hz, $^4J_{5/3}$ = 2.0 Hz); 8.13 (2H, m, H_{2Pbpy} + H_{6Pbpy}); 8.01 (2H, td, H_{4T} + $H_{4''T}$, $^3J_{4/3}$ = $^3J_{4/5}$ = $^3J_{4''/3''}$ = $^3J_{4''/5''}$ = 7.9 Hz, $^4J_{4/6}$ = $^4J_{4''/6''}$ = 1.5 Hz); 7.81 (2H, d, H_{6T} + $H_{6''T}$, $^3J_{6/5}$ = $^3J_{6''/5''}$ = 5.5 Hz); 7.75 (2H, m, $H_{2'Pbpy}$ + $H_{6'Pbpy}$); 7.38 (2H, m, H_{5T} + $H_{5''T}$); 7.30–7.21 (4H, m, $H_{6'B}$ + $H_{5'B}$ + H_{3Pbpy} + H_{5Pbpy}); 7.05 (2H, m, $H_{3'Pbpy}$ + $H_{5'Pbpy}$); 3.95 (3H, s, OCH_3); 3.83 (3H, s, OCH_3).

[Ru(MPterpy)(MP$_2$bipy)(CH$_3$CN)](PF$_6$)$_2$. ^{1}H NMR (CD_3CN, 400 MHz): δ 9.60 (1H, d, H_{6B}, $^3J_{6/5}$ = 6.0 Hz); 9.00 (1H, m, H_{3B}, $^4J_{3/5}$ = 2.1 Hz); 8.83 (2H, s, $H_{3'T}$ + $H_{5'T}$); 8.74 (1H, m, $H_{3'B}$); 8.61 (2H, m, H_{3T} + $H_{3''T}$); 8.23 (1H, dd, H_{5B}, $^3J_{5/6}$ = 6.0 Hz, $^4J_{5/3}$ = 2.0 Hz); 8.16 (4H, m, H_{2Pt} + H_{6Pt} + H_{2Pb} + H_{6Pb}); 8.07 (2H, td, H_{4T} + $H_{4''T}$, $^3J_{4/3}$ = $^3J_{4/5}$ = $^3J_{4''/3''}$ = $^3J_{4''/5''}$ = 7.9 Hz, $^4J_{4/6}$ = $^4J_{4''/6''}$ = 1.5 Hz); 7.85 (2H, d, H_{6T} + $H_{6''T}$, $^3J_{6/5}$ = $^3J_{6''/5''}$ = 5.5 Hz); 7.78 (2H, m, $H_{2'Pb}$ + $H_{6'Pb}$); 7.40 (2H, m, $H_{6'B}$ + $H_{5'B}$); 7.34–7.27 (6H, m, H_{5T} + $H_{5''T}$ + H_{3Pt} + H_{5Pt} + H_{3Pb} + H_{5Pb}); 7.08 (2H, m, $H_{3'Pb}$ + $H_{5'Pb}$); 3.99 (3H, s, OCH_3); 3.98 (3H, s, OCH_3); 3.86 (3H, s, OCH_3).

Computational details

The four ruthenium–nitrosyl complexes were fully optimized using the Gaussian-09 program package[24] within the framework of Density Functional Theory (DFT). In all cases, the calculations were performed in the presence of acetonitrile, which was modelled using the Polarizable Continuum Model (SCRF = PCM method).[25] The double-ζ basis set 6-31G* was used for all atoms except the heavy ruthenium atom, for which the LANL2DZ basis set was applied to account for relativistic effects.[26] We have selected the hybrid functional B3PW91 for the optimization, for better coherency with previous investigations. Indeed, B3PW91 has been shown to outperform other hybrid functionals (*e.g.* B3LYP) and pure functionals (*e.g.* PW91) in numerous cases of ruthenium complexes,[27] especially when back bonding ligands (like NO) are present.[28] In our previous investigation of $[RuT1B0]^{3+}$,[18c] several functionals were tested for the calculations of the UV-visible spectra (B3PW91, B3LYP, PBE0, and CAM-B3LYP) by time-dependent (TD)-DFT. CAM-B3LY[29] was finally selected, for its better accuracy to reproduce the experimental transition energies (<0.5 eV in all cases). Using the same conditions was found to be satisfactory here as well. The computed geometries of FT, and *cis*- and *trans*-$[Ru^{II}(FT)Cl_2(NO)]^+$ are provided as ESI† with the details of the related UV-visible computed spectra.

Photochemical investigations

Photochemistry. Kinetic studies on the photolysis reactions were carried out with a diode array Hewlett Packard 8452A spectrophotometer. Solutions of 2 mL of $[RuT0B2](PF_6)_3$ (2.33×10^{-5} mol L^{-1} for irradiation at 365 nm) and $[RuT1B2](PF_6)_3$ (3.75×10^{-5} mol L^{-1} for irradiation at 436 nm) in non-deoxygenated acetonitrile were used. The optical fiber was fixed laterally to the cuvette. Absorption spectra were taken after each 3 minutes, in fast scan mode, during a period of 21 hours, which allows reaching apparently stable absorption conditions. The UV-vis spectra were recorded under irradiation realized with a Muller reactor device equipped with a cooling water filter and a mercury arc lamp equipped with an appropriate interference filter to isolate the desired irradiation wavelength (λ_{max} = 365 nm or 436 nm). The temperature was maintained at 25 °C during the whole experiment.

Quantum yield measurements. Light intensities were determined before each photolysis experiment by a chemical actinometry procedure. The actinometers used were potassium ferrioxalate at λ_{irr} = 436 nm ($I_0 = 2.59 \times 10^{-7}$ mol L^{-1} s^{-1}), and at λ_{irr} = 365 nm ($I_0 = 5.30 \times 10^{-6}$ mol L^{-1} s^{-1}). The quantum yield (ϕ_A) was determined by the program Sa3.3 written by D. Lavabre and V. Pimienta.[30] It allows one to solve the following differential equation:

$$\frac{d[A]}{dt} = -\Phi_A I_a^A = -\Phi_A \, Abs_A^{\lambda} I_0 F \qquad (2)$$

where I_a^A is the intensity of the light absorbed by the precursor, Abs_A^{λ} the absorbance before irradiation, Abs_{Tot}^{λ} the total absorbance, I_0 the incident intensity measured at 436 nm, and F the photo-kinetic factor given defined as:

$$F = \frac{\left(1 - 10^{-Abs_{Tot}^{\lambda}}\right)}{Abs_{Tot}^{\lambda}} \qquad (3)$$

Eqn (2) was fitted with the experimental data $Abs_{Tot}^{\lambda} = f(t)$ and 2 parameters ϕ_A and ε_B (ε_B is the molar extinction coefficient measured at the end of the reaction) at two wavelengths (λ_{irr} = 436 nm, λ_{obs} = 470 nm for $[RuT1B2](PF_6)_3$; λ_{irr} = 365 nm, λ_{obs} = 420 nm for $[RuT0B0](PF_6)_3$ and λ_{irr} = 365 nm, λ_{obs} = 470 nm for $[RuT0B2](PF_6)_3$). λ_{obs} was chosen because it corresponds to a large difference between the molar extinction coefficient at the initial and final time of the photochemical reaction. Simulation and optimization procedures were performed by using numerical integration and a non-linear minimization algorithm for fitting of the model to the experimental data.[30,31] It has to be pointed out that ϕ_{NO} was previously published elsewhere for $[RuT1B0](PF_6)_3$.[18c] Nevertheless, we have found that this previous value was overestimated due to a wrong evaluation of I_0. Contrary to the previous study, the pH of the solution was carefully lowered by addition of sulfuric acid in the actinometry procedure in the present case, thus leading to a better evaluation of I_0 and a concomitant reduction of ϕ_{NO}. The experimental data reported here are all based on this new procedure.

Data for $[RuT0B0](PF_6)_3$

$[A]_0 = 8.66 \times 10^{-5}$ mol L^{-1}, ε_A^{365} = 7500 mol^{-1} L cm^{-1}, ε_A^{420} = 577 mol^{-1} L cm^{-1}, ε_B^{365} = 2246 mol^{-1} L cm^{-1}, ε_B^{420} = 6813 mol^{-1} L cm^{-1}.

Data for $[RuT0B2](PF_6)_3$

$[A]_0 = 2.33 \times 10^{-5}$ mol L^{-1}, ε_A^{365} = 31 759 mol^{-1} L cm^{-1}, ε_A^{470} = 3527 mol^{-1} L cm^{-1}, ε_B^{365} = 14 116 mol^{-1} L cm^{-1}, ε_B^{470} = 180 58 mol^{-1} L cm^{-1}.

Data for $[RuT1B2](PF_6)_3$

$[A]_0 = 3.76 \times 10^{-5}$ mol L^{-1}, ε_A^{436} = 17 872 mol^{-1} L cm^{-1}, ε_A^{470} = 8318 mol^{-1} L cm^{-1}, ε_B^{436} = 15 131 mol^{-1} L cm^{-1}, ε_B^{470} = 20 126 mol^{-1} L cm^{-1}.

Electrochemical studies

Electrochemical experiments were performed with a potentiostat Autolab PGSTAT100 (EcoChemie, The Netherlands) controlled by GPES 4.09 software. Experiments were carried out at room

temperature in a homemade airtight three-electrode cell connected to a vacuum/argon line. The reference electrode was a saturated calomel electrode (SCE) separated from the solution by a bridge compartment. The counter electrode was a platinum wire of *ca.* 1 cm^2 apparent surface area. The working electrode was a Pt microdisk (radius = 0.25 mm). The supporting electrolyte (nBu4N)(PF6) (Fluka, 99% electrochemical grade) was used as received and simply degassed under argon. Acetonitrile was freshly purified prior to use. The solutions used during the electrochemical studies were 10^{-3} mol L^{-1} and 10^{-1} mol L^{-1} respectively for the ruthenium complexes and for the supporting electrolyte. Before each measurement, the solutions were degassed by bubbling argon through them, and the working electrode was polished with a polishing machine (Presi P230). Typical instrumental parameters for recorded square wave voltammograms were: SW frequency f = 20 Hz, SW amplitude E_{sw} = 20 mV, and scan increment dE = 5 mV. The irradiation performed prior to recording the voltammograms of the photoproducts was performed with a mercury lamp. The voltammograms for the new $[RuT0B2](PF_6)_3$ and $[RuT1B2](PF_6)_3$ compounds and the complete redox potentials tables along the $[RuT0B0](PF_6)_3$, $[RuT1B0](PF_6)_3$, $[RuT0B2](PF_6)_3$, $[RuT1B2](PF_6)_3$ series are provided as ESI.†

Results and discussion

Synthesis and characterization

The synthesis of $[RuT0B2](PF_6)_3$ and $[RuT1B2](PF_6)_3$ reported here follows the general route previously reported for $[RuT1B0](PF_6)_3$ which implies the introduction of the ruthenium atom as $Ru^{III}Cl_3$ followed by that of the nitrosyl ligand through a first reaction of nitrite (NO_2^-) switched to NO^+ in acidic medium.[18c] This synthetic procedure avoids the production of a large amount of undesirable homoleptic $[Ru^{II}(terpy)_2]^{2+}$ species which was observed when Ru(NO) is introduced with the $[Ru^{II}Cl_5(NO)]^{2-}$ reagent.[32]

Contrary to the synthesis of related complexes built up from unsubstituted bipyridines,[18] the first step of the present synthesis (Scheme 2) requires the use of the rather insoluble MP_2bipy, which led to unexpected difficulties. Eventually, the reactions were successfully achieved in ethylene glycol, following a procedure previously used in our group in the case of ruthenium nitrosyl complexes with insoluble ligands.[33] The use of an excess of triethylamine (TEA) is justified at this step to facilitate the reduction of Ru^{III} to Ru^{II} according to a mechanism previously suggested,[34,35] which implies electron transfer from TEA to the hexacoordinated ruthenium center without direct binding. Additionally, we have observed in most cases that a $[Ru^{III}(terpy)(bipy)X]$ complex undergoes spontaneous $Ru^{III} \rightarrow Ru^{II}$ reduction, even in the absence of a clear reducing agent (*vide infra*). In the case of $[RuT1B2](PF_6)_3$, the substitution of NO_2^- for Cl^- required a purification step as previously reported by Snow *et al.*[22] The reaction steps 2 and 3 in Scheme 2 are easily monitored by ^{1}H-NMR spectroscopy, from the observation of the shift of one proton located in position 6 on the bipyridine, spatially close to the monodentate ligands (Cl, NO_2 or NO), and therefore subject to their deshielding influence. Thereby, switching from –Cl to $–NO_2$ substituents and subsequently to –NO leads to the peak-shifting of the proton in position 6 from 10.18 ppm (in CD_3CN) to 9.82 ppm (in CD_3CN) and finally to 9.23 ppm (in CD_3CN) in the case of $[RuT0B2](PF_6)_3$ and from 10.20 ppm (in CD_3OD) to 9.87 ppm (in CD_3CN) and finally to 9.23 ppm (in CD_3CN) in the case of $[RuT1B2](PF_6)_3$.

Applying two-dimensional NMR-techniques HMBC, HMQC and COSY allows the complete assignment of the peaks observed in ^{1}H- and ^{13}C-NMR spectra for the four diamagnetic Ru(Cl), $Ru(NO_2)$, and Ru(NO)-based species. The stretching vibrations (ν_{NO}) are observed at 1933 cm^{-1} and 1937 cm^{-1} for $[RuT1B2](PF_6)_3$, and $[RuT0B2](PF_6)_3$, respectively. These values fall close to those of 1940 cm^{-1} and 1944 cm^{-1} previously recorded in $[RuT1B0](PF_6)_3$,[18c] and $[RuT0B0](PF_6)_3$.[33] Nevertheless, a tendency for decreasing frequencies is apparent when the number of methoxyphenyl donating substituent increases. This observation is in complete agreement with the idea that increasing the donating capabilities of the complexes gradually increases the charge transfer towards the antibonding π^* level of the withdrawing nitrosyl, and reduces its bond order and eventually its stretching frequency.

Optical properties

The UV-visible spectra recorded in acetonitrile are compared in Fig. 1 for the four compounds under investigation. At first glance, a rough tendency for higher intensity is observed as the size of the π-skeleton of the ligands increases, from $[RuT0B0](PF_6)_3$ to $[RuT1B2](PF_6)_3$. More precisely, and apart from high energy transitions in the 250–300 nm range having likely $\pi \rightarrow \pi^*$ intra-ligand character, two main features are observed at about 375 nm and at about 425 nm. The transition at 375 nm is present in the four complexes, with a tendency for higher intensity in the species containing the MP_2bipy ligand. The transition at 425 nm of weaker intensity is present in species containing the MPterpy ligand, only. Interestingly, the UV-visible spectrum of $[RuT1B2](PF_6)_3$ seems to result grossly from the sum of that of $[RuT1B0](PF_6)_3$, and that of $[RuT0B2](PF_6)_3$. This observation suggests that, to a large extent, the origin of the electronic transition at 425 nm is roughly the same for both $[RuT1B2](PF_6)_3$, and $[RuT0B2](PF_6)_3$. This idea is further developed by DFT analysis.

DFT analyses

Before discussing the computed optical properties, it is interesting to comment on the evolution of a few relevant data from the ground

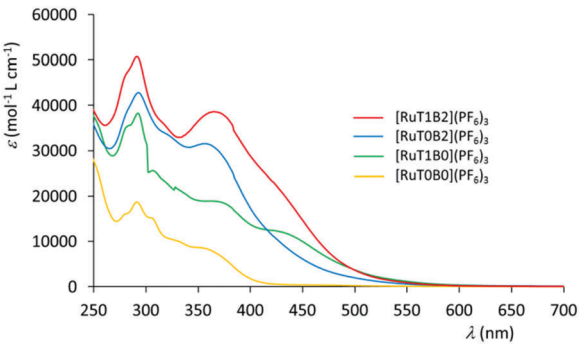

Fig. 1 Comparison of the UV-visible spectra of the ruthenium complexes, in acetonitrile.

Table 1 Relevant data for the DFT-computed ruthenium nitrosyl complexes in the ground state: NO bond length (d_{NO} in Å), NO stretching frequency (ν_{NO} in cm^{-1}), and torsion angle between the methoxyphenyl and the related pyridine rings (α in °)

				α	
Compound	MP	d_{NO}	ν_{NO}	MP-terpy	MP_2-bipy
$[RuT0B0]^{3+}$	0	1.132	2054		
$[RuT1B0]^{3+}$	1	1.134	2043	28.81	
$[RuT0B2]^{3+}$	2	1.133	2045		26.70(t)[a] and 28.28(c)[b]
$[RuT1B2]^{3+}$	3	1.135	2033	29.13	27.09(t)[a] and 28.57(c)[b]

[a] Methoxyphenyl on the pyridine in the *trans* position with respect to the Ru(NO). [b] Methoxyphenyl on the pyridine in the *cis* position with respect to the Ru(NO).

state optimizations in order to evaluate the charge transfer features along the [Ru(NO)] series. They are gathered in Table 1.

As previously discussed, the charge transfer effects on NO (increasing d_{NO}, and decreasing ν_{NO} values) are more pronounced when the number of MP donor units increases. Nevertheless, the opposite is observed for the donating counterparts. Indeed, the MP to pyridine charge transfer is reduced (increasing torsion angle) when the number of donors increases from 0 to 3. This evolution is readily understood from the fact that the withdrawing capability of a single NO is distributed on several donors, thus leading to a reduction of the effect on each individual donor. Additionally, the data gathered in Table 2 suggest that the effect of one substitution achieved on the terpyridine ligand is as efficient as that of two substitutions achieved on the bipyridine. A similar behavior has previously been observed in our group for a fluorenyl-based Ru(NO) complex.[33]

The TD-DFT computed spectra are compared in Fig. 2 for the four $[RuT0B0]^{3+}$, $[RuT1B0]^{3+}$, $[RuT0B2]^{3+}$, and $[RuT1B2]^{3+}$ complexes. Although some discrepancies are apparent in general between the theoretical and experimental spectra, it is possible to point out a few computational features supporting the experimental data: (i) the tendency for higher overall intensity as the size of the π-skeleton of the ligands increases is evidenced in full agreement with the experiment; (ii) the presence of a sizeable low-lying transition at $\lambda > 400$ nm is observed only for the complexes in which a donor is present on the terpyridine (MPterpy); and (iii) the spectrum of $[RuT1B2]^{3+}$ seems to result from the sum of those of $[RuT1B0]^{3+}$ and $[RuT0B2]^{3+}$, in the low-lying 375–425 nm wavelength domain. More precisely, the transitions at 413 nm and 382 nm computed for $[RuT1B2]^{3+}$ seem to correspond to those computed at 417 nm and 394 nm for $[RuT1B0]^{3+}$ and $[RuT0B2]^{3+}$, respectively. The detailed analysis of these transitions is provided in Table 2, to check this hypothesis.

The data gathered in Table 2 lead to the suggestion that the two dominant transitions of $[RuT1B2]^{3+}$ ($1 \rightarrow 5$ and $1 \rightarrow 7$) are reminiscent of those of $[RuT1B0]^{3+}$ ($1 \rightarrow 3$) and $[RuT0B2]^{3+}$ ($1 \rightarrow 5$), respectively. Indeed, they are found to possess roughly the same energies, relative intensities and charge transfer properties. The comparison of these transitions is further depicted at the molecular level in Fig. 3. It allows concluding unambiguously that the two transitions present in $[RuT1B2]^{3+}$ are those of the parent $[RuT1B0]^{3+}$ and $[RuT0B2]^{3+}$ species without any significant mixing. This absence of mixing can be tentatively related to the symmetries of the orbitals involved in the transitions.

Within the assumption of an ideal octahedral RuN_6 coordination sphere, schematized in Scheme 3, the terpyridine ligand appears to lie in the *XZ* plane and the bipyridine ligand to lie in the *XY* plane. In $[RuT1B0]^{3+}$, the dominant $1 \rightarrow 3$ transition possesses $\pi_{Y(terpy)}$ to $d_{XY}\pi_X^*$ character, while the dominant $1 \rightarrow 5$ transition of $[RuT0B2]^{3+}$ possesses $\pi_{Z(bipy)}$ to $d_{YZ}\pi_Z^*$ character. Both charge transfer phenomena being strictly orthogonal, it is therefore not surprising that they found their counterpart in $[RuT1B2]^{3+}$, without any mixing.

$NO^{\bullet}$ photo-release from $[RuT1B0](PF_6)_3$, $[RuT0B2](PF_6)_3$ and $[RuT1B2](PF_6)_3$

Numerous ruthenium nitrosyl complexes have been observed to release $NO^{\bullet}$ under irradiation, with very different quantum yields, depending on the nature of the ligands. For example, in the case of $[Ru(bipy)_2L(NO)]^{2-3+}$ complexes, Da Silva *et al.* reported a ϕ_{NO} value of 0.98 when $L = Cl^-$.[12] This value drops to 0.17 with L = 4-picoline and furthermore to 0.07 with L = 4-acetylpyridine.[12] In $[Ru(terpy)L(NO)]^{3+}$ complexes, $\phi_{NO} = 0.14$ when L = bipy, but rises to 0.46 when L is an orthophenylenediamine.[17] The authors relate these evolutions to the withdrawing character of the L ligand, which hampered efficient Ru → NO charge transfer, assuming that this charge transfer is the dominant parameter to account for the $NO^{\bullet}$ release.

Clearly ruthenium–nitrosyl complexes with polypyridyl ligands possess a very broad range of possible ϕ_{NO} values. However, the mechanism responsible for the release process was never unambiguously established. According to theoretical analyses by Mascharak, the release is ascribed in all cases to the

Table 2 Details of the low energy transitions involved in the TD-DFT computed spectra of the ruthenium–nitrosyl complexes: absorption maxima (λ_{max}), oscillator strengths (*f*), composition of the configuration interactions (CI), and characters

Compound	Transition	λ_{max} (nm)	*f*	CI expansion[a]	Main character
$[RuT0B0]^{3+}$	$1 \rightarrow 7$	345	0.058	59% $\chi_{116\rightarrow117}$ + 14% $\chi_{112\rightarrow117}$	terpy → Ru(NO)
	$1 \rightarrow 10$	324	0.042	88% $\chi_{115\rightarrow118}$	bipy → Ru(NO)
$[RuT1B0]^{3+}$	$1 \rightarrow 3$	417	0.227	76% $\chi_{144\rightarrow145}$	$MP_{(terpy)}$ → Ru(NO)
$[RuT0B2]^{3+}$	$1 \rightarrow 3$	434	0.029	33% $\chi_{172\rightarrow174}$ + 32% $\chi_{166\rightarrow174}$	$MP_{(bipy)}$ + bipy → Ru(NO)
	$1 \rightarrow 5$	393	0.276	47% $\chi_{171\rightarrow174}$ + 31% $\chi_{172\rightarrow174}$	$MP_{(bipy)}$ → Ru(NO)
$[RuT1B2]^{3+}$	$1 \rightarrow 5$	413	0.269	65% $\chi_{198\rightarrow201}$	$MP_{(terpy)}$ → Ru(NO)
	$1 \rightarrow 7$	382	0.359	37% $\chi_{199\rightarrow202}$ + 36% $\chi_{200\rightarrow202}$	$MP_{(bipy)}$ → Ru(NO)

[a] Orbitals 116 (117), 144 (145), 172 (173), and 200 (201) are the HOMO (LUMO) in $[RuT0B0]^{3+}$, $[RuT1B0]^{3+}$, $[RuT0B2]^{3+}$, and $[RuT1B2]^{3+}$, respectively.

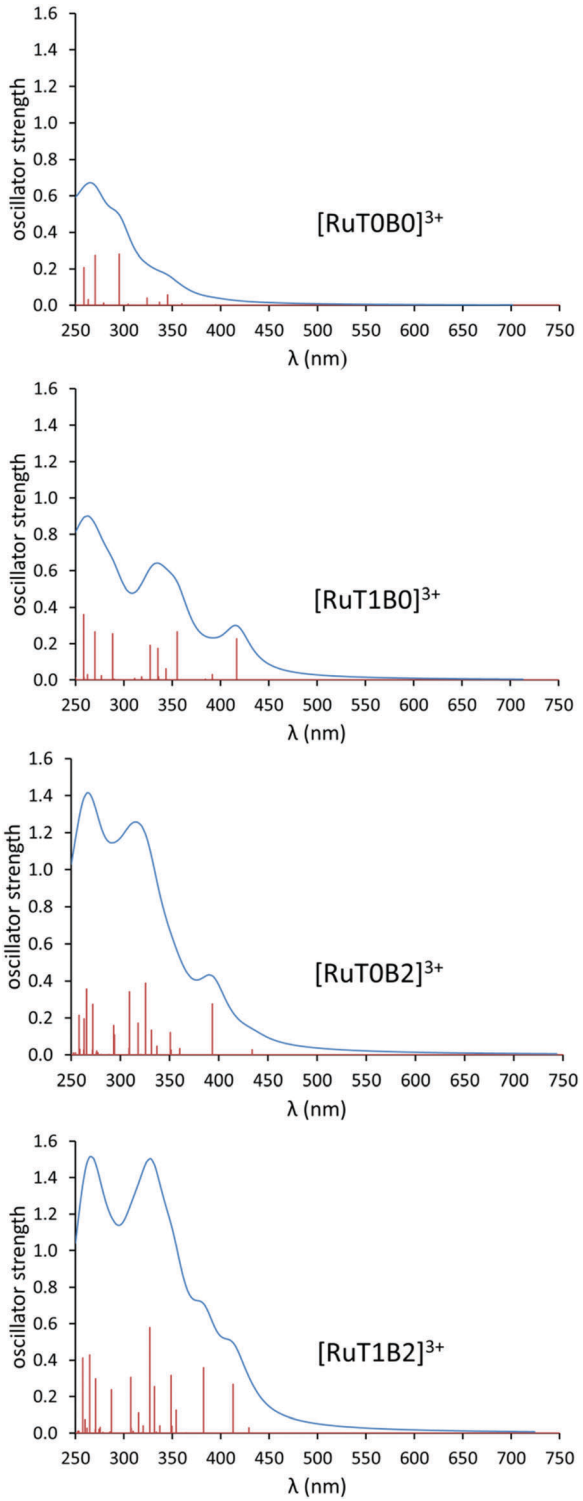

Fig. 2 Comparison of the UV-visible spectra computed at the CAM-B3LYP/6-31G* level for the ruthenium nitrosyl complexes.

population of an excited state having strong d_{Ru}–π_{NO}* antibonding character.[3a,36] Interestingly, the associated transitions tend towards the overall process depicted in eqn (1), which leads to: (i) electron transfer to NO^+ which is switched to $NO^\bullet$, (ii) weakening of the Ru–NO bond and finally, (iii) $NO^\bullet$ release supporting a mechanism in one step. Apart from this simple picture, different dissociation mechanisms have been suggested with a first excitation towards an additional ligand, however still followed by conversion to the antibonding d_{Ru}–π_{NO}* excited state.[36–38] Recently, molecular dynamics beyond the Born–Oppenheimer approximation has been used to point out the possibility of intersystem crossing towards a triplet state susceptible to undergoing additional excitation towards higher triplet states or isomerization to a metastable bent conformation prior to the $NO^\bullet$ releasing.[9,39] The use of multiconfigurational wave functions has also been proposed to provide a better description of the bonding properties of Ru(NO) metal complexes.[40] These proposed mechanisms should further be tested by experimental data to support the computational suggestions, although it is difficult to compare experiments conducted on different species at different wavelength irradiation, owing to the number of potential parameters to be taken into account.

A recent investigation in our group has come to the conclusion that the quantum yield of photo-release (ϕ_{NO}) is hardly correlated with the donating capabilities of the ligands, along a series of substituted $[Ru(R\text{-terpy})Cl_2(NO)]^+$ complexes.[41] However, the irradiation was performed at a constant wavelength on these complexes in which the absorption maxima, and the nature and the number of the involved transitions were variable, thus hampering reliable conclusions to be established. By contrast, we present here an evaluation of ϕ_{NO} at λ = 436 nm in $[RuT1B0](PF_6)_3$ and $[RuT1B2](PF_6)_3$, which undergo the same transition at this wavelength, selected among our set of filters available as the most suitable for this investigation. First, the deconvolution of the UV-visible spectra in the low energy domain (Fig. 4) is examined to verify the effect of the irradiation on the different species. The wavelengths of the de-convoluted transitions are compared to the TD-DFT data in Table 3, to verify the reliability of the analysis. In the case of $[RuT1B0](PF_6)_3$, the transition at 425 nm is the only one active under irradiation at 436 nm. By contrast, the deconvolution reveals the presence of three transitions (λ = 340 nm, 369 nm, and 421 nm) in closer proximity in $[RuT1B2](PF_6)_3$, so the resulting shape shows a shoulder at the irradiation wavelength. Nevertheless, it appears that about 90% of the light provided at 436 nm is used to promote the transition at 421 nm (Fig. 4, bottom). It can therefore be concluded that, to a large extent, the behaviors of $[RuT1B2](PF_6)_3$ and $[RuT1B0](PF_6)_3$ should be identical under this irradiation. By contrast, the deconvolution clearly reveals that the irradiation has to be conducted around λ = 350 nm in $[RuT0B2](PF_6)_3$, for the only intense transition observed at low-energy. More precisely, λ = 365 nm was selected as corresponding to the most suitable wavelength in our set of filters available.

The change in the electronic absorption spectrum of $[RuT1B2](PF_6)_3$ in acetonitrile, under irradiation at λ = 436 nm, is shown in Fig. 5. It reveals the presence of isosbestic points at λ = 222, 266, 348 and 442 nm, which indicate a clean conversion of the $Ru^{II}(NO^+)$ complexes to the related photolysed species. No back-reaction is observed when the light is turned off. In the resulting photo-product, new bands arise at 282, 312, and 476 nm. Similar experiments were conducted on $[RuT1B0](PF_6)_3$ at 436 nm

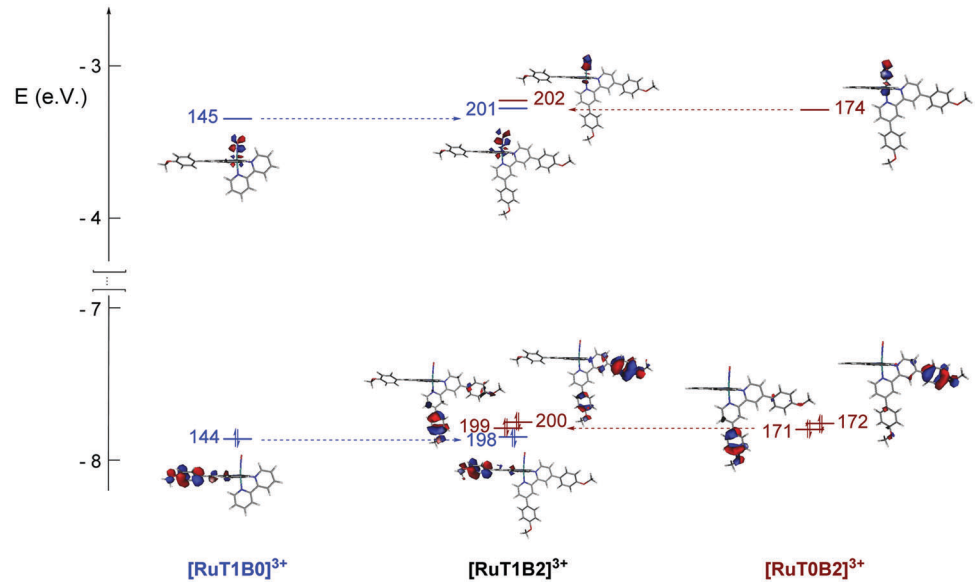

Fig. 3 Main orbitals involved in the dominant low-energy transitions of $[RuT1B0]^{3+}$, $[RuT0B2]^{3+}$, and $[RuT1B2]^{3+}$.

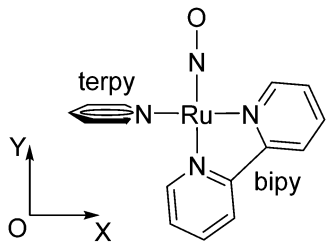

Scheme 3 Partial coordination sphere in the *XY* plane for a [Ru(terpy)-(bipy)(NO)]$^{3+}$ species in the case of ideal RuN_6 octahedral symmetry.

and on $[RuT0B2](PF_6)_3$ at 365 nm (see ESI†). Moreover, the three photoproducts exhibit rather similar UV-visible spectroscopic features with a transition in the 450–500 nm domain and a multi-transition band located between 250 and 350 nm.

It is worth pointing out that the shape of the UV-visible spectra of the photoproducts (red curve in Fig. 5 and Fig. S7 in ESI†) does not exhibit the large and broad band centered at 600 nm characteristic of Ru^{III}, which is predicted by eqn (1). This might suggest that NO is released as NO^+ rather than $NO^\bullet$. However, this hypothesis has to be abandoned after the examination of the EPR spectra recorded under irradiation in the presence of $[Fe^{II}(MGD)_2]$ which behaves as a powerful spin trapping reagent and leads to the observation of a stable spin adduct exhibiting the characteristic triplet signal of $NO^\bullet$ (Fig. 6). These behaviors are exemplified here for $[RuT0B2](PF_6)_3$, in Fig. 6, with a hyperfine splitting constant value of $a_N = 1.21 \times 10^{-3}$ cm^{-1} and a *g*-factor equal to 2.040, values which are fully consistent with reports found in the literature for $[Fe^{II}(MGD)_2$-NO] adducts.[23] Note that the residual signal observed without irradiation (upper part of Fig. 6) is related to the fact that experiments are never strictly conducted in the dark.

Eventually, the observation of a ruthenium(II) complex as the stable final photoproduct is not so surprising. Indeed, we have observed that, after $NO^\bullet$ release, the expected $[Ru^{III}(solvent)]^{3+}$ complex is invariably reduced to Ru^{II}, in the case of complexes in which 5 pyridines are present in the coordination sphere, so $[Ru^{II}(solvent)]$ is the only observable species arising after the $NO^\bullet$ release.[18] A previous investigation has pointed out the unexpected appearance of nitrates in the crystal structure of the Ru^{II} photoproduct of RuNO complexes containing 5 pyridines. This leads to the suggestion of $NO^\bullet$ as the potential reducing agent in the fast reduction process.[18c] Indeed, one third of the released $NO^\bullet$ available could be used to reduce the photoproducts, as described below:

$$Ru^{III} \xrightarrow{+1e} Ru^{II} \quad (4)$$

$$1/3NO^\bullet \xrightarrow{-1e} 1/3NO_3^- \quad (5)$$

No other investigations were carried out to elucidate the nature of the reducing agent accounting for the fast reduction process.

The presence of Ru^{II} instead of Ru^{III} after irradiation is further confirmed by electrochemistry, with the appearance of an oxidation wave after irradiation along the RuNO series, the values of which are gathered in Table 4. Interestingly, the oxidation becomes more favorable (shifted to lower potentials) as the number of donating substituents increases, in agreement with chemical intuition. A similar effect is evidenced before irradiation with the $NO^+ \rightarrow NO^\bullet$ wave shifted to lower potential indicating that it becomes more difficult to reduce the species having more donating substituents. Altogether the spectroscopic and electrochemical data lead to the conclusion that, although the nature of the reducing agent is not clearly established, eqn (1) has to be re-written as follows:

$$\begin{aligned}[Ru^{II}(NO^+)] + \text{solvent} &\xrightarrow{h\nu} [Ru^{III}(\text{solvent})] + NO^\bullet \\ &\xrightarrow{\text{fast}} [Ru^{II}(\text{solvent})] + NO^\bullet\end{aligned} \quad (6)$$

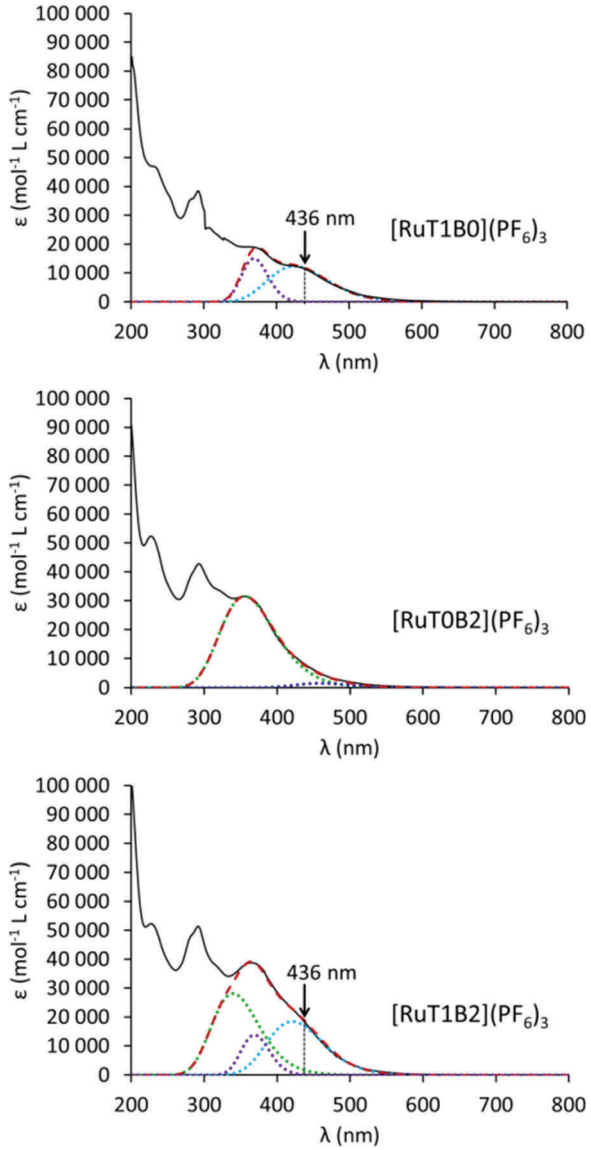

Fig. 4 UV-visible spectra of $[RuT1B0](PF_6)_3$, $[RuT0B2](PF_6)_3$, and $[RuT1B2](PF_6)_3$ (black solid lines) with deconvolutions: the red dashed lines are the sum of the contribution of dotted lines (see text).

Table 3 Comparison of the de-convoluted (left) and computed (right) transitions in the UV-visible spectrum of $[RuT1B0](PF_6)_3$, $[RuT0B2](PF_6)_3$, and $[RuT1B2](PF_6)_3$: data in blue are ascribed to T1 → RuNO transitions and data red to B2 → RuNO transitions

Experimental data		TD-DFT computation	
Compound	Deconvoluted transition	Compound	Transition
$[RuT1B0](PF_6)_3$	425 nm	$[RuT1B0]^{3+}$	417 nm
	369 nm		355 nm
$[RuT0B2](PF_6)_3$	458 nm (weak)	$[RuT0B2]^{3+}$	434 nm (weak)
	356 nm		393 nm
$[RuT1B2](PF_6)_3$	421 nm	$[RuT1B2]^{3+}$	413 nm
	369 nm		382 nm
	340 nm		349 nm

Finally, the ϕ_{NO} values obtained by treatment of the time dependence of the absorbance of the intense low-energy transitions

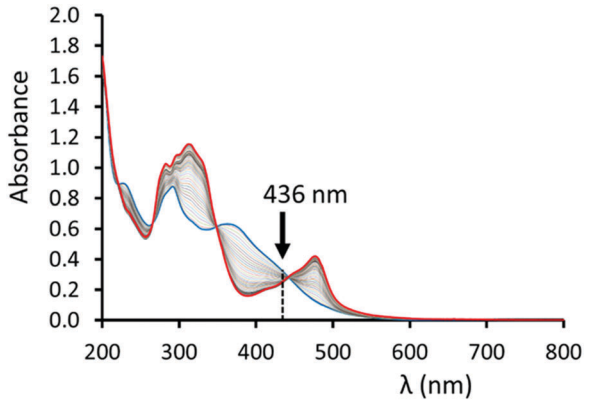

Fig. 5 Changes in the absorption spectrum of $[RuT1B2](PF_6)_3$, in acetonitrile, under irradiation at λ = 436 nm. The blue curve corresponds to the starting complex and the red curve corresponds to the photo-product.

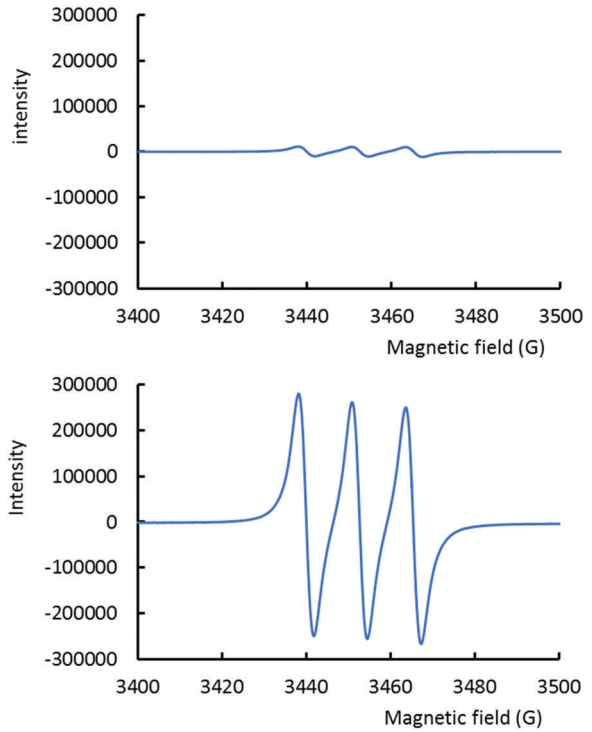

Fig. 6 Representative triplet signal from $NO^{\bullet}$ trapped by $[Fe^{II}(MGD)_2]$ in acetonitrile, after irradiation of $[RuT0B2](PF_6)_3$ with a Hg lamp (bottom). The signal recorded before irradiation is given as a reference (top).

of $[RuT1B0](PF_6)_3$, $[RuT0B2](PF_6)_3$, and $[RuT1B2](PF_6)_3$ are shown in Table 5. Surprisingly, and while the transitions arise from the same general MP → RuNO charge transfer behavior in all cases, their associated ϕ_{NO} values scale from 0.002 to 0.024, in a ratio of 1 to 12. More precisely, the experiments conducted under the same irradiation conditions (λ = 436 nm) on $[RuT1B2](PF_6)_3$ and $[RuT1B0](PF_6)_3$ lead to ϕ_{NO} values of 0.002 and 0.011, respectively, in a ratio 1 to 6, contrary to the expectation of unvarying properties arising from identical (MP-terpy → RuNO) charge transfer transitions. This striking difference forces us to recognize that the simple one step (transition → release) mechanism cannot

Table 4 Selected redox potentials (*vs.* SCE electrode) observed in the square-wave voltammograms of $[RuT0B0](PF_6)_3$, $[RuT1B0](PF_6)_3$, $[RuT0B2](PF_6)_3$, and $[RuT1B2](PF_6)_3$

Compound	Before irradiation $NO^+/NO^\bullet$	After irradiation Ru^{III}/Ru^{II}
$[RuT0B0](PF_6)_3$	0.47	1.29
$[RuT1B0](PF_6)_3$	0.44[a]	1.27[a]
$[RuT0B2](PF_6)_3$	0.42	1.23
$[RuT1B2](PF_6)_3$	0.39	1.20

[a] Data from ref. 12*c*.

account for the observation of such different properties. It has therefore to be inferred that the singlet excited state promoted after one-photon absorption cannot release $NO^\bullet$ spontaneously.

Alary *et al.* have recently proposed that, in $[Ru^{II}(terpy)Cl_2(NO)]^+$ complexes, the Ru–NO bond cannot be broken in the singlet excited state, but is rather switched to a triplet state by an intersystem crossing reaction.[9] Furthermore, this triplet could be subject to evolution towards a bent Ru–N–O intermediate, the so called MS2 state, which is subject to additional photon absorption, and finally, to the release of nitric oxide. A two-photon mechanism was recently evidenced in the RuNO/RuON photo-isomerization of $[Ru(py)_4Cl(NO)](PF_6)_2$, a reaction which frequently competes with the photorelease and implies first the breaking of the ruthenium–nitrosyl bond.[42] Owing to this observation, the issue of a possible sequential two-photon mechanism along the present RuNO series cannot be avoided.

To the best of our knowledge, the requirement for a second photon and the need for a triplet state mechanism were never proven experimentally in the release process. In the present case, the requirement for an intermediate (*e.g.* MS2) species is not verified experimentally, due to the presence of isosbestic points in Fig. 5 which favors a simple two-species (A → B) mechanism. If it is involved here, MS2 must necessarily be extremely photo-reactive, so its concentration stays very weak throughout the entire release process. Although this possibility cannot be strictly dismissed, we clearly have no experimental data in hand suggesting that this two-photon mechanism takes place in our compounds.

As a final comment, it is worth pointing out that the photoproduct generated under irradiation of $[RuT1B2](PF_6)_3$ undergoes significant absorption at 436 nm (Fig. 5). As a consequence the completion of the photo-release process required a long irradiation time of about 40 hours. Under these conditions, the issue of possible additional photoreactions of the photoproduct with dissociation of the chelating ligands could have been considered. Indeed, release of bidentate π-acceptors ligands, such as bipyridine, has been observed under irradiation in some cases.[43–46] Nevertheless, a set of experimental features allow us to exclude this possibility as a significant behavior: (i) isosbestic points in the UV-vis spectra revealing the presence of a single photoproduct; (ii) photochemical analysis applied satisfactorily on the basis of a single photoproduct, (iii) a lack of NO in the photoproduct confirmed by EPR and IR spectroscopy, and (iv) finally the presence of a single photoproduct monitored by ^1H NMR spectroscopy.

Table 5 Quantum yield of $NO^\bullet$ photo release (ϕ_{NO}) after irradiation (λ_{irr}) of the intense low-energy transition (λ_{max}) of $[RuT0B0](PF_6)_3$, $[RuT1B0](PF_6)_3$, $[RuT0B2](PF_6)_3$, and $[RuT1B2](PF_6)_3$

Compound	λ_{max} (nm)	λ_{irr} (nm)	ϕ_{NO}
$[RuT0B0](PF_6)_3$	352	365	0.086
$[RuT1B0](PF_6)_3$	425	436	0.011
$[RuT0B2](PF_6)_3$	356	365	0.024
$[RuT1B2](PF_6)_3$	421	436	0.002

Conclusion

The report of the new $[RuT0B2](PF_6)_3$, and $[RuT1B2](PF_6)_3$ compounds allowed us to obtain a series of four ruthenium nitrosyl complexes built up from the $[Ru(terpy)(bipy)(NO)]^{3+}$ core with 0, 1, 2, and 3 methoxyphenyl donating units. Computational DFT analysis conducted in support of the experimental data leads to a comprehensive report of the role of the charge transfer effects in both ground and excited states with low-energy transitions arising from methoxyphenyl to ruthenium nitrosyl charge transfer, in all cases. Despite these similarities, irradiation performed on these transitions leads to $NO^\bullet$ photorelease with significantly different quantum yields, in the broad 0.002–0.02 range. More precisely, and due to orbital orthogonality, the low energy transitions are found to be identical in $[RuT1B0](PF_6)_3$ and $[RuT1B2](PF_6)_3$, nevertheless, with different quantum yields in a ratio of 1 to 6. This unexpected result proves that the intuitive mechanism based on a simple "absorption + release" scheme is unable to account for the experimental data. More sophisticated models are required either by introducing very reactive intermediates or intersystem conversion to hypothetical triplet states, as suggested by theory. Additional experimental data are necessary to clarify if more than one photon is required to release $NO^\bullet$ in these species.

Conflicts of interest

There are no conflicts to declare.

Acknowledgements

The authors wish to thank Dr Alix Sounia-Saquet (LCC-CNRS) for performing the electrochemical experiments, Lionel Rechignat (LCC-CNRS) for his assistance with EPR experiments, and Dr Isabelle Sasaki (ISM-Bordeaux) for helpful discussions. M. R. thanks the Ministère de l'Enseignement Supérieur et de la Recherche (MESR) for a PhD fellowship.

References

1 L. J. Ignarro, *Nitric oxide biology and pathobiology*, Academic Press, San Diego, 1st edn, 2000.
2 S. Singh and A. K. Gupta, *Cancer Chemother. Pharmacol.*, 2011, **67**, 1211–1224.

3 (*a*) N. L. Fry and P. K. Mascharak, *Acc. Chem. Res.*, 2011, **44**, 289–298; (*b*) M. J. Rose and P. K. Mascharak, *Coord. Chem. Rev.*, 2008, **252**, 2093–2114.
4 For recent reports on NO• release from ruthenium nitrosyl complexes, see: (*a*) M. Guo, H. J. Xiang, Y. Wang, Q. L. Zhang, L. An, S. P. Yang, Y. Ma, Y. Wang, J. G. Liu and J. Gang, *Chem. Commun.*, 2017, **53**, 3253–3256; (*b*) G. L. S. Rodrigues and W. R. Rocha, *J. Phys. Chem. B*, 2016, **120**, 11821–11833; (*c*) N. Cacita, B. Possato, C. F. N. da Silva, C. M. Paulo, A. L. B. Formiga, L. M. Bendhack and S. Nikolaou, *Inorg. Chim. Acta*, 2015, **429**, 114–121; (*d*) J. C. M. Pereira, M. L. Souza and D. W. Franco, *Eur. J. Inorg. Chem.*, 2015, 1005–1011; (*e*) K. Ghosh, R. Kumar, K. Kumar, A. Ratnam and U. P. Singh, *RSC Adv.*, 2014, **4**, 43599–43605; (*f*) M. S. P. Marchesi, S. A. Cicillini, A. C. L. Prazias, L. M. Bendhack, A. A. Batista and R. S. Silva, *Transition Met. Chem.*, 2012, **37**, 475–479.
5 J. H. Enemark and R. D. Feltham, *Coord. Chem. Rev.*, 1974, **13**, 339–406.
6 R. D. Feltham and J. H. Enemark, *Topics in Stereochemistry*, ed. G. Geoffroy, J. Wiley & Sons, New York, 1981, vol. 12, p. 155.
7 G. K. Lahiri and W. Kaim, *Dalton Trans.*, 2010, **39**, 4471–4478.
8 A. P. de Lima Batista, A. G. S. de Oliveira-Filho and S. E. Galembeck, *Phys. Chem. Chem. Phys.*, 2017, **19**, 13860–13867.
9 J. S. Garcia, F. Alary, M. Boggio-Pasqua, I. M. Dixon and J.-L. Heully, *J. Mol. Model.*, 2016, **22**, 284.
10 G. L. S. Rodrigues and W. R. Rocha, *J. Phys. Chem. B*, 2016, **120**, 11821–11833.
11 L. Freitag and L. Gonzalez, *Inorg. Chem.*, 2017, **53**, 6415–6426.
12 (*a*) R. Galvao de Lima, M. Gama Sauaia, C. Ferezin, I. Muniz Pepe, N. M. Jose, L. M. Bendhack, Z. Novais da Rocha and R. Santana da Silva, *Polyhedron*, 2007, **26**, 4620–4624; (*b*) M. G. Sauaia, R. Galvao de Lima, A. C. Tedesco and R. Santana Da Silva, *J. Am. Chem. Soc.*, 2003, **125**, 14718–14719; (*c*) M. G. Sauaia, F. de Souza Oliveira, A. C. Tedesco and R. Santana Da Silva, *Inorg. Chim. Acta*, 2003, **355**, 191–196; (*d*) V. Togniolo, R. Santana da Silva and A. C. Tedesco, *Inorg. Chim. Acta*, 2001, **316**, 7–12.
13 (*a*) F. O. N. Silva, M. C. L. Candido, A. K. M. Holanda, I. C. N. Diogenes, E. H. S. Sousa and L. G. F. Lopes, *J. Inorg. Biochem.*, 2011, **105**, 624–629; (*b*) F. O. N. Silva, S. X. B. Araujo, A. K. M. Holanda, E. Meyer, F. A. M. Sales, I. C. N. Diogenes, I. M. M. Carvalho, I. S. Moreira and L. G. F. Lopes, *Eur. J. Inorg. Chem.*, 2006, 2020–2026.
14 E. C. Fornari, M. S. P. Marchesi, A. E. H. Machado and S. Nikolaou, *Polyhedron*, 2009, **28**, 1121–1126.
15 (*a*) A. D. Chowdhury, P. De, S. M. Mobin and G. K. Lahiri, *RSC Adv.*, 2012, **2**, 3437–3446; (*b*) P. De, B. Sarkar, S. Maji, A. K. Das, E. Bulak, S. M. Mobin, W. Kaim and G. K. Lahiri, *Eur. J. Inorg. Chem.*, 2009, 2702–2710; (*c*) S. Maji, B. Sarkar, M. Patra, A. K. Das, S. M. Mobin, W. Kaim and G. K. Lahiri, *Inorg. Chem.*, 2008, **47**, 3218–3227.
16 H. Giglmeier, T. Kerscher, P. Kluefers, D. Schaniel and T. Woike, *Dalton Trans.*, 2009, 9113–9116.
17 R. Galvao de Lima, M. Gama Sauaia, D. Bonaventura, A. C. Tedesco, L. M. Bendhack and R. Santana da Silva, *Inorg. Chim. Acta*, 2006, **359**, 2543–2549.
18 (*a*) A. Enriquez-Cabrera, I. Sasaki, V. Bukhanko, M. Tassé, S. Mallet-Ladeira, P. G. Lacroix, R. M. Barba-Barba, G. Ramos, N. Farfán, Z. Voitenko and I. Malfant, *Eur. J. Inorg. Chem.*, 2017, 1446–1456; (*b*) A. Enriquez-Cabrera, P. G. Lacroix, I. Sasaki, S. Malet-Ladeira, N. Farfan, R. M. Barba-Barba, G. Ramos-Ortiz and I. Malfant, *Eur. J. Inorg. Chem.*, 2018, 531–543; (*c*) V. Bukhanko, P. G. Lacroix, I. Sasaki, M. Tassé, S. Mallet-Ladeira, Z. Voitenko and I. Malfant, *Inorg. Chim. Acta*, 2018, **482**, 195–205.
19 (*a*) W. R. Murphy Jr., K. Takeuchi, M. H. Barley and T. J. Meyer, *Inorg. Chem.*, 1986, **25**, 1041–1053; (*b*) D. W. Pipes and T. J. Meyer, *Inorg. Chem.*, 1984, **23**, 2466–2472.
20 E. C. Constable, C. E. Housecroft, M. Neuburger, I. Poleschak and M. Zehnder, *Polyhedron*, 2003, **22**, 93–108.
21 Y. Chen, W. Guo, Z. Ye, G. Wang and J. Yuan, *Chem. Commun.*, 2011, **47**, 6266–6268.
22 P. A. Adcock, F. Richard Keene, R. S. Smythe and M. R. Snow, *Inorg. Chem.*, 1984, **23**, 2336–2343.
23 A. J. Liu, Q. Duan, J. Wang, Z. Song, X. Qiao and H. Wang, *J. Biomed. Opt.*, 2015, **20**(1), 015004.
24 M. J. Frisch, G. W. Trucks, H. B. Schlegel, G. E. Scuseria, M. A. Robb, J. R. Cheeseman, G. Scalmani, V. Barone, B. Mennucci, G. A. Petersson, H. Nakatsuji, M. Caricato, X. Li, H. P. Hratchian, A. F. Izmaylov, J. Bloino, G. Zheng, J. L. Sonnenberg, M. Hada, M. Ehara, K. Toyota, R. Fukuda, J. Hasegawa, M. Ishida, T. Nakajima, Y. Honda, O. Kitao, H. Nakai, T. Vreven, J. A. Montgomery, Jr., J. E. Peralta, F. Ogliaro, M. Bearpark, J. J. Heyd, E. Brothers, K. N. Kudin, V. N. Staroverov, R. Kobayashi, J. Normand, K. Raghavachari, A. Rendell, J. C. Burant, S. S. Iyengar, J. Tomasi, M. Cossi, N. Rega, J. M. Millam, M. Klene, J. E. Knox, J. B. Cross, V. Bakken, C. Adamo, J. Jaramillo, R. Gomperts, R. E. Stratmann, O. Yazyev, A. J. Austin, R. Cammi, C. Pomelli, J. W. Ochterski, R. L. Martin, K. Morokuma, V. G. Zakrzewski, G. A. Voth, P. Salvador, J. J. Dannenberg, S. Dapprich, A. D. Daniels, Ö. Farkas, J. B. Foresman, J. V. Ortiz, J. Cioslowski and D. J. Fox, *Gaussian 09, Revision D.01*, Gaussian, Inc., Wallingford CT, 2009.
25 J. Tomasi, B. Mennucci and R. Cammi, *Chem. Rev.*, 2005, **105**, 2999–3093.
26 (*a*) P. J. Hay and W. R. Wadt, *J. Chem. Phys.*, 1985, **82**, 270–283; (*b*) W. R. Wadt and P. J. Hay, *J. Chem. Phys.*, 1985, **82**, 284–298; (*c*) P. J. Hay and W. R. Wadt, *J. Chem. Phys.*, 1985, **82**, 299–310.
27 For example: (*a*) M. P. Waller, H. Braun, N. Hojdis and M. Bühl, *J. Chem. Theory Comput.*, 2007, **3**, 2234–2242; (*b*) T. Ayed, J. C. Barthelat, B. Tangour, C. Pradère, B. Donnadieu, M. Grellier and S. Sabo-Etienne, *Organometallics*, 2005, **24**, 3824–3826; (*c*) H. Hratchian and M. C. Milleti, *J. Mol. Struct. THEOCHEM*, 2005, **340**, 119–126; (*d*) D. Huang, W. E. Streib, O. Eisenstein and K. G. Caulton, *Organometallics*, 2000, **19**, 1967–1972.
28 P. Hirva, M. Haukka and M. Jaconen, *J. Mol. Model.*, 2008, **14**, 171–181.
29 T. Yanai, D. Tew and N. Handy, *Chem. Phys. Lett.*, 2004, **393**, 51–57.

30 D. Lavabre and V. Pimienta, Program Sa3.3, http://cinet.chim.pagesperso-orange.fr/tele_sa/install_Sa.html.
31 V. Pimienta, C. Frouté, M.-H. Deniel, D. Lavabre, R. Guglielmetti and J. C. Micheau, *J. Photochem. Photobiol., A*, 1999, **122**, 199–204(ref. 35).
32 J. Akl, Ch. Billot, P. G. Lacroix, I. Sasaki, S. Malet-Ladeira, I. Malfant, R. Arcos-Ramos, M. Romero and N. Farfan, *New J. Chem.*, 2013, **37**, 3518–3527.
33 M. Roose, I. Sasaki, V. Bukhanko, S. Mallet-Ladeira, R. M. Barba-Barba, G. Ramos-Ortiz, A. Enriquez-Cabrera, N. Farfan, P. G. Lacroix and I. Malfant, *Polyhedron*, 2018, **151**, 100–111.
34 K. Abbas and D. Marji, *Z. Naturforsch., A: Phys. Sci.*, 2005, **60**, 667–671.
35 F. Kanoufi, Y. Zu and A. J. Bard, *J. Phys. Chem. B*, 2001, **105**, 210–216.
36 N. L. Fry and P. K. Mascharak, *Dalton Trans.*, 2012, **41**, 4726–4735.
37 A. C. Merkle, N. L. Fry, P. K. Mascharak and N. Lehnert, *Inorg. Chem.*, 2011, **50**, 12192–21203.
38 W. Zheng, S. Wu, S. Zhao, Y. Geng, J. Jin, Z. Su and Q. Fu, *Inorg. Chem.*, 2012, **51**, 3972–3980.
39 L. Freitag and L. González, *Inorg. Chem.*, 2014, **53**, 6415–6426.
40 A. P. de Lima Batista, A. G. S. de Oliveira-Filho and S. E. Galembeck, *Phys. Chem. Chem. Phys.*, 2017, **19**, 13860–13867.
41 S. Amabilino, M. Tasse, P. G. Lacroix, S. Mallet-Ladeira, V. Pimienta, J. Akl, I. Sasaki and I. Malfant, *New J. Chem.*, 2017, **41**, 7371–7383.
42 L. Khadeeva, W. Kaszub, M. Lorenc, I. Malfant and M. B.-L. Cointe, *Inorg. Chem.*, 2016, **55**, 4117–4123.
43 L. M. Loftus, K. F. Al-Afyouni, F. Kathlyn and C. Turro, *Chem. – Eur. J.*, 2018, **24**, 11550–11553.
44 D. Havrylyuk, D. K. Heidary, L. Nease, S. Parkin and E. C. Glazer, *Eur. J. Inorg. Chem.*, 2017, 1687–1694.
45 E. Wachter, D. K. Heidary, B. S. Howerton, S. Parkin and E. C. Glazer, *Chem. Commun.*, 2012, **48**, 9649–9651.
46 A. C. Laemmel, J. P. Collin and J. P. Sauvage, *Eur. J. Inorg. Chem.*, 1999, 383–386.